1 **Air pollution reductions caused by the COVID-19 lockdown open up a way to preserve**

2 **the Himalayan Glaciers**

4 Suvarna Fadnavis[1*], Bernd Heinold[2], T. P Sabin[1], Anne Kubin[2], Katty Huang[3], Alexandru

5 Rap[4], and Rolf Müller[5]

6 [1]Indian Institute of Tropical Meteorology, Centre for climate change research, Ministry of
7 Earth Sciences, India

8 [2]Leibniz-Institut für Troposphärenforschung, Leipzig, Germany,

9 [3]Urban Climate, Risk & Health, UCL, London, United Kingdom

10 [4]School of Earth and Environment, University of Leeds, Leeds, UK,

11 [5]Forschungszentrum Jülich GmbH, IEK-7, Jülich, Germany,

12 Corresponding author email: suvarna@tropmet.res.in

13 Abstract

14 The rapid melting of glaciers in the Hindu Kush Himalayas (HKH) during recent decades poses

15 an alarming threat to water security for larger parts of Asia. If this melting persists, the entire

16 Himalayan glaciers are estimated to disappear by end of the 21st century. Here, we assess the

17 influence of the spring 2020 COVID-19 lockdown on the HKH, demonstrating the potential

18 benefits of a strict emission reduction roadmap. Chemistry-climate model simulations,

19 supported by satellite and ground measurements, show that lower levels of gas and aerosol

20 pollution during lockdown led to changes in meteorology, and to a reduction in black carbon

21 in snow (2-14%) and thus in snow melting (10-40%). This caused increases in snow cover (6-

22 12%) and mass (2-20%) and a decrease in runoff (5-55%) over the HKH and Tibetan Plateau,

23 ultimately leading to an enhanced snow-equivalent-water (2–55%). We emphasize the

24 necessity for immediate anthropogenic pollution reductions to address the hydro-climatic threat

25 to billions of people in South Asia.

26

1.   Introduction

The Hindu Kush Himalayan (HKH) mountains and Tibetan plateau is the largest snow-cladded region outside the Poles (Fig. 1). This region is also referred to as High Mountain Asia, although that includes the Tien Shan and some other northern ranges. The HKH meltwater feeds rivers in India and China that drive the agriculture, hydropower generation, and economy of these countries (Hussain et al., 2019; Sabin et al., 2020; Lee et al. 2021a). The Himalayan snowmelt in spring provides ~50% of the annual freshwater to ~4 billion people of South Asia and East Asia (Sarangi et al 2019, Sabin et al., 2020). Rapid Himalayan snowmelt caused a loss of ~40 % of the Himalayan glacier area compared to the Little Ice Age, 400 to 700 years ago, i.e. ~0.92 to 1.38 mm sea-level equivalent (Lee et al., 2021b). The snow mass over the Himalayas has generally decreased during the last 30 years (except for a few Karakoram glaciers that show an increasing trend in snow mass) (Hussain et al., 2019. The alarming rate of snow melting of 0.02 to 0.6 cm $^{\circ}C^{-1}$ day^{-1} raised concerns about the sustainability of water supply (Tiwari et al., 2015) and loss of glaciers in the region (Hussain et al., 2019, Lee et al., 2021b). Model simulations for extreme scenarios show that Himalaya snow melting could cause the glaciers to disappear by the end of the 21st century (Cruz et al. 2007, Hock et al., 2019).
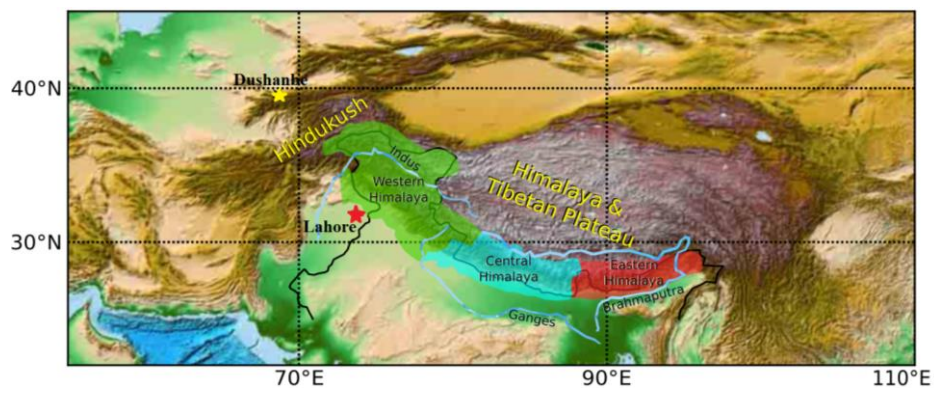
Figure 1: Map of the Hindu Kush Himalayas region with the Western (70 - 80º E, 30º - 35º N), Central (80º - 87º E, 28º - 30º N), and Eastern Himalayas (88º - 95º E, 26º - 30º N). A yellow and red star indicates the location of the AERONET sun photometer stations Dushanbe (68.858º E, 38.553 º N) and Lahore (74.264º E, 31.480º N), respectively.

The accelerated thinning of Himalayan glaciers is attributed to climate change causing shifts in air temperature and precipitation, as well as the atmospheric distribution and deposition of light-absorbing particles i.e., dust and black carbon (BC) (IPCC Climate Change 2013, Krishnan et al., 2019). Among the aforementioned factors, snow darkening due to the deposition of absorbing aerosols is an integral component of Himalayan snowmelt and runoff (Lau et al., 2010). The snow-melting efficacy of BC is higher than that of greenhouse gases (Qian et al., 2011; Nair et al. 2013; Ma et al., 2019; Sarangi et al., 2019). The increasing energy demand of the densely populated South Asian region has increased the emission of greenhouse gases and BC aerosol in the last few decades (Fadnavis et al., 2017, Krishnan et al., 2020), leading to enhanced darkening and snow melting (Usha et al., 2021).

The economic slowdown caused by the COVID-19 pandemic measures led to a drastic reduction in public and freight transportation, industrial emissions, and energy use (Fadnavis et al., 2021a). This resulted in a substantial decline in emissions of several atmospheric pollutants including greenhouse gases and black carbon aerosol (Forster et al. 2020; Kanniah et al., 2020; Le Quéré et al 2020), and potentially reduced deposition of dark aerosols on snow and ice (Bair et al., 2021). Remote sensing approaches show cleaner snow with ~30% less light-absorbing impurities in snow during the lockdown period over Asia between March and May 2020 (Bair et al 2021). This led to decreased snowmelt by 25 – 70 mm in 2020 compared to the last 20-year mean for March-May over Western Himalayas due to decreased radiative forcing induced by BC and dust deposition on snow/ice surfaces and related changes in snow absorption and surface albedo (Bair et al., 2021). Bair et al. (2021) also found that 6.6 km^{-3} of melt water stayed in the Indus Basin. Gauge and reservoir data for this part of the world, however, are not freely available. Impacts of reduced levels of air pollution on changes in the snow mass, surface water runoff, and water reservoir over the HKH are not reported hitherto.

77 Here, we provide a detailed analysis of the impact of reduced pollution over HKH and Tibetan

78 plateau region during the COVID-19 lockdown period between March and May 2020. We used

79 global simulations with the chemistry-climate model ECHAM6-HAMMOZ (Schultz et al.,

80 2018, Tegen et al., 2019), updated with an improved BC-in-snow parameterization (Huang

81 2018), in order to contrast the 2020 COVID-19 (COVID) with the typical, unchanged (control,

82 CTL) air pollution conditions. The COVID simulations are performed using a COVID-19

83 emission inventory where emissions are reduced based on Google and Apple mobility data

84 (Forster et al., 2020; details in section S1).

85

86 **2   Results**

87 **2.1 Reduction of airborne aerosols and in-snow BC concentration over the Himalayas**
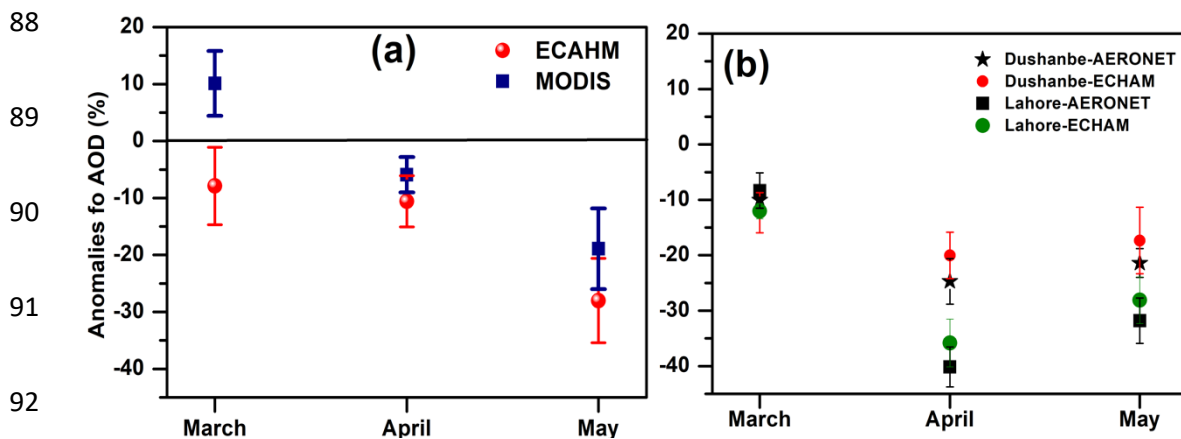
93 **Figure 2:** (a) Changes in monthly mean AOD (%) during March - May 2020 from MODIS in
94 comparison to mean of 2001-2019 and ECHAM-HAMMOZ (COVID minus CTL) averaged
95 over the Hindu Kush Himalayas (HKH) and Tibetan Plateau region (75º - 95º E, 30º - 35º N),
96 (b) same as (a) but for AOD from AERONET observations and ECHAM-HAMMOZ model
97 results at Dushanbe (68.858º E, 38.553º N, climatology 2010-2019) and Lahore (74.264º E,
98 31.480º N, climatology 2006-2019). Vertical bars in Fig (a)-(b) indicate the standard deviation
99 within ten members of model simulations, and within monthly mean anomalies from MODIS
100 for years 2001-2019.

101

102   The COVID-19 lockdown restrictions in spring 2020 decreased the anthropogenic

103   aerosol amounts over the HKH ranges (Western, Central, and Eastern Himalayas), and the

104   Tibetan Plateau region. The ECHAM6-HAMMOZ model simulations show that COVID

105   lockdown resulted in a cleaner atmosphere during March - May 2020 over the HKH ranges and

106   Tibetan Plateau region. There is a reduced level of Aerosol Optical Depth (AOD) over the

107   region throughout spring 2020 by -8.1±6.2 % in March, -10.2±4.7% in April, -27±6.9 % in

108   May compared to the CTL (non COVID) simulation (Fig. 2a). This is supported by NASA's

109   Moderate Resolution Imaging Spectroradiometer (MODIS) measurements also showing a

110   reduction in AOD in April (-5.6±3.3%) and May (-18.8±7.2%) 2020 compared to the mean

111   over the last 20 years (Fig. 2a). Thus, both model simulations and MODIS AOD show a

112   reduction in aerosol pollution in April - May 2020. For March 2020, MODIS measurements

113   show AOD enhancement by 10.2 ±4.8 %, which is due to increased dustiness over the HKH

114   region (see section S2 for a detailed discussion). AOD measurements at two Aerosol Robotic

115   Network (AERONET) sun photometer stations in Dushanbe (68.858º E, 38.553º N)

116   and Lahore (74.264º E, 31.480º N) show an AOD reduction in agreement with our model

117   simulations (Fig. 2b). There are differences among MODIS, AERONET and the model. The

118   changes in AOD during COVID compared to no-COVID period is less in the model than the

119   MODIS observations by 4.2 - 9.8 % and higher than the AERONET observations by 1.8 - 4.2

120   %. These differences are due to the fact that the simulated AOD change is in response to the

121   reduction of anthropogenic aerosols and associated circulation responses, while MODIS and

122   AERONET measurements show the effect of all atmospheric processes. Also, note that the

123   MODIS AOD values are spatial averages representative for a relatively large area while the

124   AERONET values are point measurements. Importantly, changes in simulated AOD in 2020

125   fall within the standard deviation of satellite and ground-based measurements indicating

126   reliability of our simulations (except for March 2020 with respect to MODIS). Our model

simulations also show a reduction in BC burden by 15 - 55% (Fig. S1a), and sulfate burden by 22 - 24 % over the HKH and Tibetan Plateau regions in spring 2020 (Fig. S1b). Interestingly, dust burden also shows a reduction over these regions (Fig. S1c, Fig. S2a-c), except over central Himalaya in March and April 2020. The lower dust load is related to the interactive change in atmospheric dynamics in the model, which also leads to changes in the wet and dry deposition rates of dust (Fig. S2d-i) (details in section S2). A drop in BC is also observed in Aerosol Radiative Forcing Over India Network (ARFINET) ground-based measurements over the Indo-Gangetic Plain (> 50 %), north-eastern India (>30%), Himalaya regions (16 - 60%), and Tibet (70%) during spring 2020 (Gogoi et al., 2021; Liu et al., 2021). A similar impact of the reduction of energy consumptions on decrease in AOD during the COVID-19 lockdown period, i.e., in spring 2020 compared to the 2010-2019 climatology is also seen over South and East Asia (40 %) and the Indo-Gangetic Plain (IGP) by 30 – 40 % in satellite measurements (Fadnavis et al., 2021a; Srivastava et al., 2021; Pandey et al., 2021; Shafeeque et al , 2021).

The reduction in anthropogenic air pollution leads widely to a reduction in BC concentration in the snow of approximately 25 - 350 μg kg^{-1} (by 12 – 35 %) during spring 2020 (Fig. 3a-c) that reduce the snow darkening effect by embedded aerosol impurities. At the most this amounts to about a 1.6% increase in visible snow albedo. Sporadically, however, the BC-in snow concentrations have also increased in some areas of the Hindukush, Eastern Himalayas and Kunlun Mountains. There are many factors at play that may lead to an increase in BC concentration in snow in some locations. For instance, this includes increases in deposition of BC following shifts in the atmospheric circulation (Fig.S3), accumulation of BC on surface snow following partial snowmelt and minimal fresh snowfall, and less frequent occurrences of complete snowmelt which would otherwise remove all accumulated BC in snow. Our simulations reveal that the decrease in BC-in snow concentration and the overall reduction in

152 atmospheric pollution, as well as associated radiative effects have decreased the shortwave

153 radiative forcing at the surface by 0.2 – 2 W m^{-2} in March – May 2020 (Fig. 3 d-f), leading to

154 a decrease in tropospheric heating by solar radiation of 0.001 to 0.015 K day^{-1} (Fig. 3 g-i). The

155 reduced anthropogenic BC over the HKH and Tibetan Plateau region resulted in less absorption

156 and re-emission of longwave radiation and, as a consequence, there is a reduction in longwave

157 radiative forcing in the atmosphere leading to a lower atmospheric heating (Fig. S4). Therefore,

158 the reduction of anthropogenic sulfate, and BC burden, combined with lower atmospheric

159 loadings of PM2.5 and PM10, as well as BC in snow resulted in decreased heating of the

160 snowpack and tropospheric column.
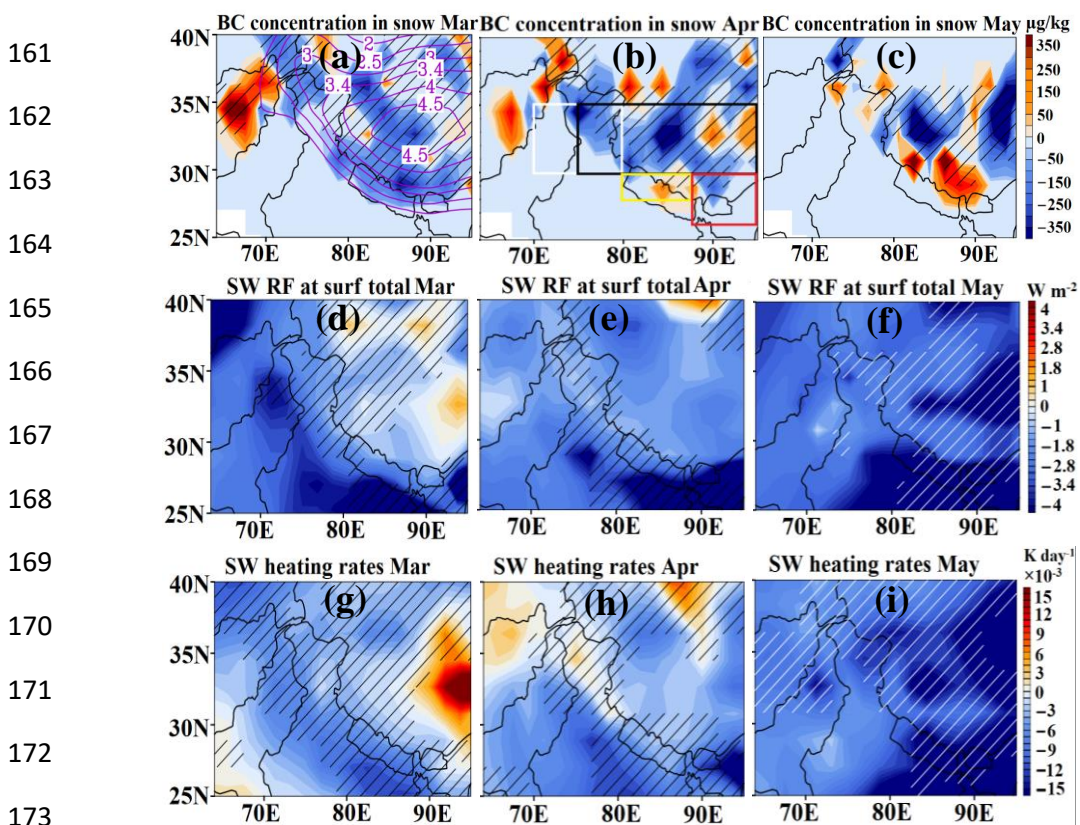
Figure 3: Spatial distribution of anomalies (COVID minus CTL) of BC concentration in snow (µg kg^{-1}) for (a) March, (b) April, and (c) May 2020; (d-f) shortwave radiative forcing (W m^{-2}) at the surface and (e-g) tropospheric heating rates (K day^{-1}) due to changes in BC concentration in snow (COVID minus CTL). Hatched areas indicate the 95%-significance level. Contours in panel (a) indicate topography in km. Boxes in panel (b) indicate boundaries of Western Himalayas (WH, white), Central Himalayas (CH, yellow), Eastern Himalayas (EH, red) and Tibetan Plateau (black).

2.2 Impacts on snow melting, surface water runoff, and snow cover

Further we show that the decrease in aerosol pollution reduced the snow melting in spring 2020 by 0.2 to 2.5 mm day^{-1} corresponding to 10 – 50 % (Fig. 4 a-c). The amount of reduction of snow melting is pronounced over the western Himalayas in May. As a result of a reduction in snowmelt, surface water runoff has been drastically reduced by 2-4 mm –ay^{-1} (5 - 55 %) (Fig. 4 d-f). The reduction in the runoff is most pronounced in May over the entire Himalayas and central Tibetan Plateau region. Estimates from remote sensing measurements also show the reduction of runoff by 6.5 km^3 of melted water in the Indus River Basin (Bair et al. 2020). In the past, studies have shown that elevated levels of light-absorbing aerosols (elemental carbon: 13 to 75 ng g^{-1} and dust: 32 to 217 µg g^{-1}) can contribute to about 3 to 10 mm day^{-1} of snowmelt over western Himalayas (Thind et al. 2019). A sensitivity analysis using a glacier mass balance model shows that a BC-induced snow albedo reduction (Fig. 4 g-i) resulted in an increase in runoff by 4 – 18% annually (Santra et al., 2019). In contrast to impacts of rising anthropogenic emissions during the past decades, emission reductions during the 2020 COVID-19 lockdown period caused a brighter snow albedo and therefore an enhanced surface reflection with albedo increases of 0.2 - 0.5 (see Fig. 4g-i), leading to less atmospheric heating as well as associated reduced snowmelt and surface water runoff in spring 2020.
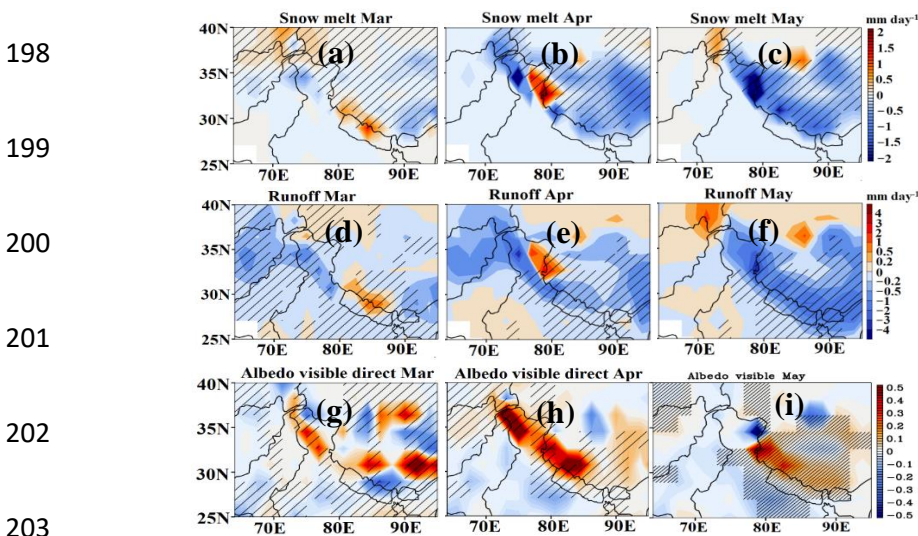
Figure 4: Spatial distribution of anomalies of (a-c) snow melt (mm day^{-1}), (d-f) surface water runoff (mm day^{-1}) for March to May 2020 (COVID minus CTL) and (g-i) surface albedo mean in the visible. Hatched areas indicate the 95%-significance level.
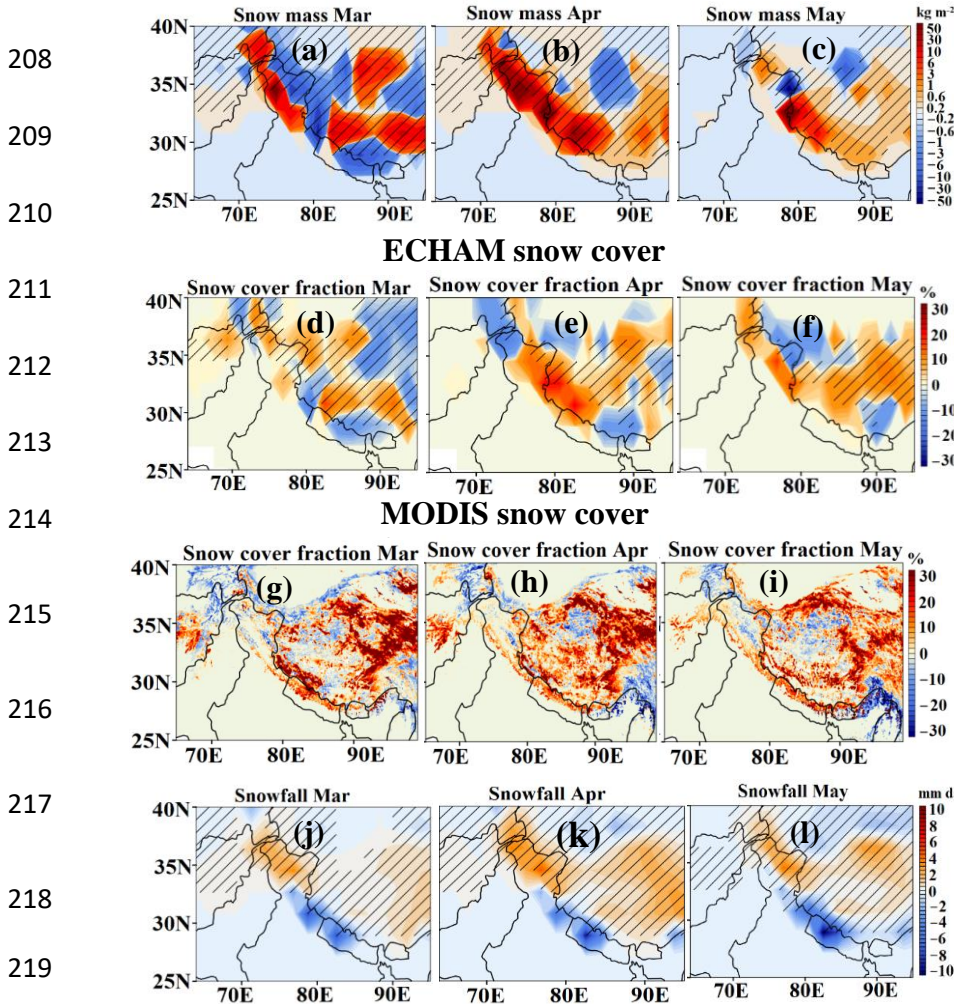
Figure 5: Monthly mean anomalies (COVID minus CTL) for March to May 2020 of (a-c) the snow mass (kg m^{-2}), (d-f) snow cover fraction (%) as modelled by ECHAM6-HAMMOZ as well as (g-i) snow cover fraction from MODIS satellite measurements (%) with respect to the climatological average 2000-2019, and, (j-l) snowfall as modelled by ECHAM6-HAMMOZ. Hatched areas indicate the 95%-significance level.

Our simulations also indicate that these changes lead to an increase in snow mass of 0.2-50 kg m^{-2}, i.e. 10-40% (Fig. 5a-c) and snow cover fraction of 2-30% during spring 2020 (Fig. 5d-f). MODIS measurements also show a remarkable agreement with the model simulations (especially during April - May 2020), with increased snow cover of about 15-30%

230   over the parts of Western Himalayas and Central Himalayas and the Tibetan Plateau region

231   and decreased by 5-12 % over parts of North-East Himalayas especially in April and May 2020

232   (Fig. 5 g-i). However, there are also some differences in terms of exact regions of snow cover

233   enhancement or reduction respectively, since the MODIS observations include the influence of

234   real-time meteorology, while meteorology in the model ensemble include internal variability

235   and do not replicate the exact conditions observed by MODIS. Our model simulations show

236   that air pollution reductions in the COVID-19 lockdown period and associated changes in

237   radiative forcing caused changes in the tropospheric circulation and thermodynamics (see

238   Fadnavis et al., 2020 for a detailed analysis). These changes in meteorology have increased

239   snowfall by 2-5 mm day^{-1} (3-20 %) over the Western Himalayas and Tibetan Plateau region

240   (Fig. 5 j-l). The increase in snowfall over these regions will contribute to enhancement in snow

241   mass and snow cover (Fig. 5 a-f) and albedo (Fig. 4 g-i). In a few areas, however, this also

242   contributes to a more efficient BC deposition on snow, as described above (Fig. 3), but this

243   does not affect the overall conclusion as to the albedo effect.

244

245   Himalaya snow is the largest source of freshwater for South Asia (Bolch et al., 2012).

246   The impact of reduced pollution on the surface water content in the Himalayas from our model

247   simulations is illustrated in Fig. 6a. The snow mass enhancement led to increase the snow

248   equivalent water by 2 to 14.7 mm (2.5 to 55 %). The western Himalayas show the highest

249   increase in snow equivalent water by 14.7 mm (55 %) followed by the Tibetan Plateau by 12

250   mm (by 22 %) and central Himalayas by 10 mm (by 18%) in April while the Eastern Himalayas

251   show a decrease in March (-1.3 mm; 10 %) and small enhancement in April by 1.1mm (2.3 %)

252   and May 2020 by 1.3 mm (2.7%) due to pollution reduction. Thus, human induced pollution

253   reduction during the COVID-19 lockdown benefitted the HKH in many ways. A schematic

254   shows the COVID-19 lockdown-induced effects in Figs. 6b-c: increased snow surface

255 reflectivity, reduced snowmelt and surface water runoff, as well as enhanced water content in

256 the reservoir and snow.
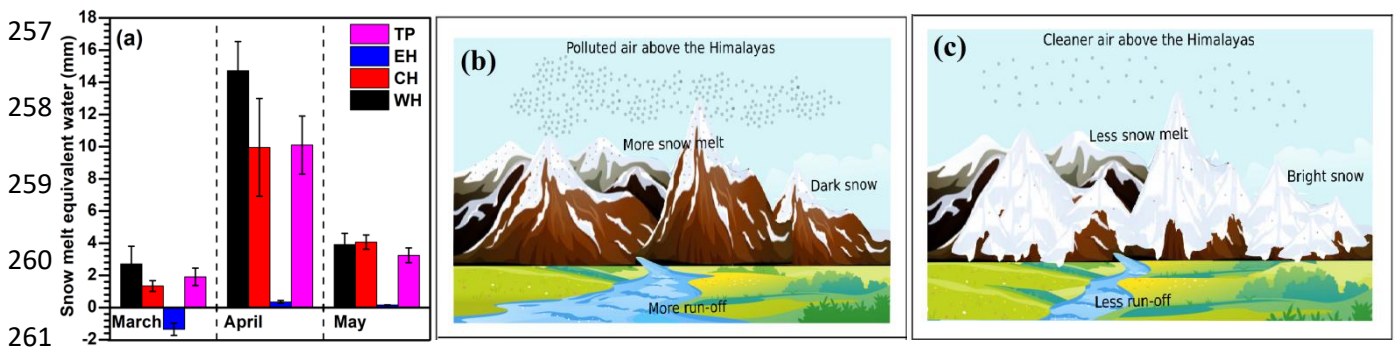
262 **Figure 6:** (a) Change in water content (mm) of the Himalayan surface reservoirs (COVID
263 minus CTL) from March to May 2020 over the Western Himalayas (WH), Central Himalayas
264 (CH), Eastern Himalayas (EH) and Tibetan Plateau (TP). Vertical bars indicate the standard
265 deviation within ten members of model simulations. Schematic illustrating the impacts of (b)
266 air pollution on snow darkening in the Himalayas and surface water runoff for the usual
267 polluted case and (c) the impacts of reduced pollution on snow brightening in the Himalayas
268 and reduced surface water runoff, as observed during the 2020 COVID-19 lockdown period.

269

270 **3.   Summary and conclusions**:   A rising trend in Asian air pollution and associated

271 climate change over the last few decades has had a detrimental impact on snow melting over

272 the Hindu Kush Himalayas (HKH) and Tibetan Plateau region (Wester et al., 2019). Black

273 carbon from increasing emissions of biomass burning, industrial and domestic combustion and

274 transport is deposited on snow, reducing its albedo (i.e. darkening) (Bolch et al., 2019). A snow

275 darkening effect, compounded with other climate change effects, accelerates the melting of

276 snow and the disappearance of ice cover over the HKH and Tibetan Plateau region at an

277 extraordinary rate (Usha et al., 2021). The drop in anthropogenic air pollution emissions, e.g.

278 from energy production, during the COVID-19 lockdown period in spring 2020 reduced air

279 pollutant levels worldwide (Forster et al., 2020). Our model simulations indicate that the

280 associated reduction in anthropogenic aerosols and greenhouse gases in spring 2020 has

281 benefited the HKH snow reservoirs. It caused an enhancement in the snow cover fraction by 6

282   - 12 % and snow mass by 2 - 20 %, corresponding to a decrease in snow melting by 10 - 40%

283   and surface water runoff by 0.2 - 3 mm day^{-1}. As a consequence, the water content of the

284   reservoir increased considerably by 4 to 59 %.

285   Our findings highlight that out of the two processes causing a retreat of Himalayan glaciers:

286   (1) a slow response to global climate change and (2) a fast response to local air pollution

287   (especially black carbon), a policy action on the latter is more likely to be within reach of

288   possible policy action on a shorter-term time scale and a more regional spatial scale. Even if

289   we stopped CO_2 emissions immediately, temperatures would not start decreasing. Our findings

290   confirm the importance of reducing short-lived climate forcers (black carbon) and their

291   complementary role to CO_2 mitigation (Rogelj et al., 2014). Reduction of air pollution to levels

292   similar with those recorded during the 2020 COVID-19 lockdown period, could safeguard

293   HKH glaciers, which are otherwise under the threat to disappear by the end of the 21st century.

294   Since 2000 Himalayan glaciers have been losing nearly half a meter of ice per year (Wester et

295   al., 2019). Our estimates indicate that air pollution reduction during COVID 19 lockdown in

296   spring 2020 caused a reduction in snow melt by 0.5 to 1.5 mm day^{-1}, indicating large benefits

297   to HKH glaciers. Even if global warming is kept below 1.5°C, one third of the glaciers in the

298   HKH region and more than half of those in the Eastern Himalaya will likely be lost by the end

299   of this century (Bolch et al., 2019). The speedily retreating glaciers and the snowpack loss are

300   already posing a threat to domestic sustainable water resources for billions of people in Asia

301   (Wood et al., 2021). However, if new economically and technically feasible policies would

302   reduce emissions of air pollutants (in particular black carbon) to at least lockdown period

303   levels, snowmelt could be reduced by 10 – 50%. Such policies will therefore bring substantial

304   benefits for sustained water supply, agriculture, and ecosystems in large parts of Asia.

305

Section S1: Methods:

S1.1 Observational data

We used monthly snow cover fraction from NASA's Moderate Resolution Imaging Spectroradiometer (MODIS) satellite product on a 0.5x0.5° resolution (version 6, level 3; Hall et al., 2006) for the years 2000 – 2020 (https://nsidc.org/data/MOD10CM/versions/6). For aerosol information we used monthly mean satellite AOD at 1x1° resolution from the MODIS Terra level-3 dark target and deep blue retrievals at 550 nm wavelength for 2001-2020 (https://giovanni.gsfc.nasa.gov). Uncertainty in MODIS AOD data over snow are documented by Huang et al (2020). We also used ground-based sun photometer observations of AOD from the Aerosol Robotic Network (AERONET) (Martonchik et al., 2004) at the stations Dushanbe (68.858º E, 38.553º N) for the period 2010-2020 and Lahore (74.264º E, 31.480º N) for the period 2006 – 2020, situated in HKH region (https://aeronet.gsfc.nasa.gov).

S1.2   The ECHAM6-HAMMOZ model description and Experimental set-up

We performed 10-member ensemble experiments using the state-of-the-art aerosol-chemistry-climate model ECHAM6-HAMMOZ (version echam6.3-ham2.3-moz1.0; Schultz et al., 2018, Tegen et al., 2019). The model comprises the atmospheric general circulation model ECHAM6 (Stevens et al., 2013), the atmospheric chemistry module MOZ (Schultz et al, 2018), and the Hamburg Aerosol Model (HAM; Stier et al., 2005; Zhang et al., 2012). The HAM component predicts the nucleation, growth, evolution, and sinks of sulphate (SO_4^{2-}), black carbon (BC), particulate organic matter (POM), sea salt (SS), and mineral dust (DU) aerosols. Seven log-normal modes describe the size distribution of the aerosol population with a prescribed variance in the aerosol module. The MOZ submodule describes the trace gas chemistry from the troposphere to the lower thermosphere. The chemical mechanism includes

330   the O_X, NO_X, HO_X, ClO_X and BrO_X chemical families, along with CH_4 and its degradation

331   products. Several primary non-methane hydrocarbons (NMHCs) and related oxygenated

332   organic compounds are also described. It contains 108 species, 71 photolytic processes, 218

333   gas-phase reactions and 18 heterogeneous reactions with aerosol (Schultz et al., 2018). Details

334   of emissions (anthropogenic, biomass burning, biogenic, fossil fuel etc.) and model

335   parametrisation and other details are reported in the past Fadnavis et al. (2017, 2019a,b, 2021b).

336   Anthropogenic and biomass burning emissions of sulphate, and black carbon (BC) and organic

337   carbon (OC) are based on the AEROCOM-ACCMIP-II emission inventory for year 2020

338   (Lamarque et al., 2010; Textor et al., 2006). Additional consideration for the reduction of snow

339   albedo due to BC in snow is implemented but extended for the MOZ module. Snow albedo

340   reduction is calculated by considering the concentration of BC in the top layer of surface snow.

341   Influxes of BC in snow include below-cloud and in-cloud wet scavenging, as well as dry

342   deposition and sedimentation. Snowmelt and glacier runoff remove the in-snow BC at a

343   reduced efficiency, leading to enhanced concentration, while fresh and pristine snowfall leads

344   to reductions in BC concentration.

345

346   The model simulations were performed at T63 horizontal resolution ($1.875° \times 1.875°$) with 47

347   levels in the vertical from the surface to 0.01 hPa (corresponding to approx. 80 km), and with

348   a time step of 20 minutes. To understand the effect of the COVID-19 restrictions on snow over

349   Himalayas and Tibetan plateau region we conducted a control (CTL) and a COVID-19

350   (COVID) simulation. We adopted an ensemble approach (with 10 ensemble members) for the

351   above two experiments. Ten spin-up simulations were performed from 1 to 31 December 2019

352   to generate stabilised initial fields for the 10 ensemble members. Emissions were the same in

353   each of the 10 members during the spin-up period. Control simulations were extended with the

354   same setup until 1 June 2020. While for the COVID simulations (10 ensemble members each),

the anthropogenic emission of all gases and aerosols were changed since 1 January 2020 according to Google and Apple mobility data as in Forster et al. (2020). The COVID-19 emissions were prepared by deriving scaling factors between the input4MIPS SSP245 baseline and the version5 of the Forster et al. (2020) 2-year blip scenario, separately for each species and each grid point (see Fig. S5a). Subsequently, these scaling factors have been applied to the AeroCom-II ACCMIP emissions. This ensures consistency of the drop in emissions independent of the absolute emission values in the AeroCom-II ACCMIP and the input4MIPS SSP245 data sets. The global mean emission changes in carbon monoxide (CO, 2-24%), black carbon (BC, 3-23%), organic carbon (OC, 2-17%), sulfur dioxide (SO_2, 3-23%), nitrogen o xides (NO_x, 2-30%), methane (CH_4, 2-5%), and ammonia (NH_3, 0-3%) during the period January to 1 July 2020 (COVID - CTL) are in agreement with previous studies Forster et al. (2020) and Le Quéré et al., (2020) (Fig. S5b). Our model experiments follow the CovidMIP protocol (Jones et al., 2021). The COVID and CTL simulations ended on 1 June 2020. To investigate the effects of COVID-19 emissions in spring (i.e., since 1 March 2020), we analysed the difference between COVID and CTL simulations for the spring season in 2020. The same dust parametrisation was employed in the CTL and COVID simulations.

A limitation of our simulation is the relatively coarse spatial resolution in the ECHAM6-HAMMOZ model (1.875°x1.875°). Other studies used a finer spatially resolved regional model; for example Sarangi et al. (2020) use a 12 x 12 km (~ 0.10°) grid in the regional WRF-Chem-SNICAR model over the same region. In our model grid of 1.875°, many of the Himalayan sub ranges are smaller than a pixel, and, hence, the topographic influences, which are substantial in the mountains are limited. One effect may be that snowfall and snow on the ground are underestimated (e.g., Liu et al., 2022). The coarse grid size can impact the anomalies found here as the changes in snow mass are small, at most +16 mm, and the bias in the likely underestimated snow mass may change between the control and COVID simulations. Biases

380   are, however, the same in the control and COVID simulations and, thus, their effects will be
381   diluted when we compute the anomalies.

382   **Section S2: Comparison of AOD over Western, Central, Eastern Himalayas and Tibetan**
383   **Plateau regions**

384   We elaborate on the comparison of MODIS AOD with our model simulations over
385   Western, Central, Eastern Himalayas and Tibetan Plateau regions (Fig. S6). Both MODIS and
386   the model show a reduction in AOD during spring 2020 over the aforementioned regions of
387   HKH. The estimated differences in AOD during March to May 2020 vary between 0.8 – 11%
388   over Western and Central Himalayas, and 8 – 16% over Eastern Himalayas. Over the Tibetan
389   plateau region, in contrast to the model simulations, MODIS shows an enhancement (2 – 16 %)
390   in AOD (Fig. S6). This may be due to dust aerosols, which are transported during spring from
391   western Asia and locally, generating dust piles over the Tibetan Plateau (Fadnavis et al., 2017,
392   2021a). The simulated dust aerosol concentration in spring 2020 over the Tibetan Plateau
393   region is smaller in the COVID than in the non-COVID (i.e. CTL) situation (Fig. S1c). The
394   changes in simulated dust are a response to meteorology difference between the COVID and
395   CTL simulations (Fig. S7).

396

397 References:

398 Bair, E., Stillinger, T., Rittger, K. & Skiles, M. COVID-19 lockdowns show reduced pollution

399 on snow and ice in the Indus River Basin. *Proc. Natl. Acad. Sci. U. S. A.* 118, 19–21,

400 https://doi.org/10.1073/pnas.2101174118, 2021. Bolch, T. *et al.* Status and Change of

401 the Cryosphere in the Extended Hindu Kush Himalaya Region. in The Hindu Kush

402 Himalaya Assessment: Mountains, Climate Change, Sustainability and People (eds.

403 Wester, P., Mishra, A., Mukherji, A. & Shrestha, A. B.) 209–255 (Springer International

404 Publishing). doi:10.1007/978-3-319-92288-1_7 2019, 2019.

405 Cruz, R.V., Harasawa, H., Lal, M., Wu, S, Anokhin, Y., Punsalmaa, B., Honda, Y., Jafari, M.,

406 Li, C., and Huu Ninh, N. Climate change 2001: impacts, adaptation, and vulnerability.

407 *Choice Rev. Online* 39, 39-3433-39–3433, 2007.

408 Fadnavis, S. Müller R., Chakraborty T., Sabin T. P., Laakso A., Rap A., Griessbach S., Vernier

409 J-P. & Tilmes S. The role of tropical volcanic eruptions in exacerbating Indian droughts.

410 *Sci. Rep.* 11, 1–13, https://doi.org/10.1038/s41598-021-81566-0, 2021.

411 Fadnavis, S., Müller R., Kalita G, Rowlinson M., Rap A., Frank Li J-L, Gasparini B, and

412 Laakso A., The impact of recent changes in Asian anthropogenic emissions of SO2 on

413 sulfate loading in the upper troposphere and lower stratosphere and the associated

414 radiative changes, ACP, 19, 9989–10008, 2019a.

415 Fadnavis, S., Sabin T. P., Roy C., Rowlinson M, Rap A, Vernier J-P.& E. Sioris C. E.. Elevated

416 aerosol layer over South Asia worsens the Indian droughts. Sci. Rep. 9, 1–12,

417 https://doi.org/10.1038/s41598-019-46704-9, 2019b.

418 Fadnavis, S., Kalita, G., Ravi Kumar, K., Gasparini, B. & Li, J. L. F. Potential impact of

419 carbonaceous aerosol on the upper troposphere and lower stratosphere (UTLS) and

420 precipitation during Asian summer monsoon in a global model simulation. *Atmos.*

421 *Chem.Phys.* 17, 11637–11654, https://doi.org/10.5194/acp-17-11637-2017, 2017.

422   Fadnavis, S.. Sabin T. P, Rap A., Müller R., Kubin A. and Heinold B., The impact of COVID-

423   19 lockdown measures on the Indian summer monsoon. *Environ. Res. Lett.* 16, DOI

424   10.1088/1748-9326/ac109c, 2021.

425   Forster, P. M. *et al.* Current and future global climate impacts resulting from COVID-19.

426   *Nat.Clim. Chang.* 10, 913–919, 2020.

427   Gogoi, M. M. S. Babu S., Arun B. S., Krishna, Moorthy K., Ajay A., Ajay P., Suryavanshi A.,

428   Borgohain A., *et al.* Response of Ambient BC Concentration Across the Indian Region

429   to the Nation-Wide Lockdown: Results from the ARFINET Measurements of ISRO-

430   GBP.*Curr. Sci.* 120, 341, doi: 10.18520/cs/v120/i2/341-351, 2021.

431   Hall, D. K. MODIS / Terra Snow Cover 5-Min L2 Swath 500m. *Color. USA NASA Natl. Snow*

432   *Ice Data Cent. Distrib. Act. Arch. Cent* 5, 2006.

433   Hock, R. *et al.* Chapter 2: High Mountain Areas. IPCC Special Report on the Ocean and

434   Cryosphere in a Changing Climate. *IPCC Spec. Rep. Ocean Cryosph. a Chang. Clim.*

435   131–202, 2019.

436   Huang, W. T. K. Aerosol effects on climate, with an emphasis on the Arctic.

437   https://doi.org/10.3929/ethz-b-000319114 2018, 2018.

438   Hussain, A. *Sarangi G.K., Pandit A., Ishaq S., Mamnun N., Ahmad B., Jamil M.K.,* Hydropower

439   development in the Hindu Kush Himalayan region: Issues, policies and opportunities.

440   *Renew. Sustain. Energy Rev.* 107, 446–461, https://doi.org/10.1016/j.rser.2019.03.010,

441   2019.

442   IPCC Working Group 1, I. *et al.* IPCC, 2013: Climate Change 2013: The Physical Science

443   Basis. Contribution of Working Group I to the Fifth Assessment Report of

444   theIntergovernmental Panel on Climate Change. *Ipcc* AR5, 1535, 2013.

445 Jones, C. D., et al. The climate response to emissions reductions due to COVID-19: Initial

446   results from CovidMIP. Geophysical Research Letters, 48, e2020GL091883.

447   https://doi.org/10.1029/2020GL091883, 2021.

448 Kanniah, K. D., Kamarul Zaman, N. A. F., Kaskaoutis, D. G. & Latif, M. T. COVID-19's

449   impact on the atmospheric environment in the Southeast Asia region. *Sci. Total*

450   *Environ.*736, 139658, https://doi.org/10.1016/j.scitotenv.2020.1396580048-9697, 2020.

451 Krishnan, R. *et al.* Assessment of climate change over the Indian region: A report of the

452   ministry of earth sciences (MOES), government of India. Assessment of Climate Change

453   over the Indian Region: A Report of the Ministry of Earth Sciences (MoES), Government

454   of India (Springer Singapore). doi:10.1007/978-981-15-4327-2, 2020.

455 Krishnan, R., Shrestha, A., Ren, G., Rajbhandari, R., Saeed, S., & Sanjay, J. Unravelling

456   Climate Change in the Hindu Kush Himalaya: Rapid Warming in the Mountains and

457   Increasing Extremes. The Hindu Kush Himalaya Assessment (Springer Singapore).

458   doi:10.1007/978-3-319-92288-1_3, 2019.1 , 2019.

459 Laakso A. The impact of recent changes in Asian anthropogenic emissions of SO2 on sulfate

460   loading in the upper troposphere and lower stratosphere and the associated radiative

461   changes.. *Atmos. Chem. Phys.* 1–44, https://doi.org/10.5194/acp-19-9989-2019, 2019a.

462 Lamarque J.-F. , Bond T. C., Eyring V., Granier C., Heil A., Klimont Z., Lee D., Liousse C.,

463   Mieville A., Owen B., Schultz M. G., Shindell D., Smith S. J., Stehfest E., Aardenne J.

464   Van, Cooper O. R., Kainuma M., Mahowald N., McConnell J. R., Naik V., Riahi K., and

465   Vuuren D. P. van, Historical (1850-2000) gridded anthropogenic and biomass burning

466   emissions of reactive gases and aerosols: Methodology and application. *Atmos. Chem.*

467   p*hys.* 10, 7017–7039, https://doi.org/10.5194/acp-10-7017-2010, 2010.

468   Lau, W. K. M., Kim, M. K., Kim, K. M. & Lee, W. S. Enhanced surface warming and

469   accelerated snow melt in the Himalayas and Tibetan Plateau induced by absorbing

470   aerosols. *Environ. Res. Lett.* 5, doi:10.1088/1748-9326/5/2/025204, 2010.

471   Le Quéré, C. *Jackson R. B., M Jones M. W., Smith A. J. P., Abernethy S. Andrew R. M. , De-*

472   *Gol A. J. Willi D. R., Shan Y., Canadell J. G., Friedlingstein P., Creutzig F. and Peters*

473   G. P., Temporary reduction in daily global CO2 emissions during the COVID-19 forced

474   confinement. *Nat. Clim. Chang.* 10, 647–653, https://doi.org/10.1038/s41558-020-0797-

475   x., 2020.

476   Lee, E., Carrivick1 J. L., Quincey D. J., Cook S. J., ames1 W. H. M., &. Brown L. E.,

477   Accelerated mass loss of Himalayan glaciers since the Little Ice Age. *Sci. Rep.* 11, 1–8,

478   https://doi.org/10.1038/s41598-021-03805-8, 2021b.

479   Lee, S. S., Chu, J. E., Timmermann, A., Chung, E. S. & Lee, J. Y. East Asian climate response

480   to COVID-19 lockdown measures in China. *Sci. Rep.* 11, 1–9, 2021a.

481   Liu, Y. *Wang Y. , Cao Y., Yang Xi, T Zhang T., Luan M., Lyu D., Hansen A. D. A., Liu B., and*

482   Liu, Y., Fang, Y., Li, D., and Margulis, S. A.: How Well do Global Snow Products Characterize

483   Snow Storage in High Mountain Asia?, Geophysical Research Letters, 49,

484   e2022GL100082, https://doi.org/10.1029/2022GL100082, 2022.

485   Ma, J. Zhang T., and GUAN X., The dominant role of snow/ice Albedo feedback strengthened

486   by black carbon in the enhanced warming over the Himalayas. *J. Clim.* 32, 5883–5899,

487   https://doi.org/10.1175/JCLI-D-18-0720.s1.2019.

488   Martonchik, J. V., Diner, D. J., Kahn, R., Gaitley, B. & Holben, B. N. Comparison of MISR

489   and AERONET aerosol optical depths over desert sites. *Geophys. Res. Lett.* 31, 1–4,

490   https://doi.org/10.1029/2004GL019807, 2004.

491   Nair, V. S. *Babu S. S,, Moorthy K. K., Sharma A. K. , Marinoni A.& Ajai,* Black carbon aerosols

492   over the Himalayas: Direct and surface albedo forcing. *Tellus, Ser. B Chem. Phys.*

493   *Meteorol.* 468 65, DOI: 10.3402/tellusb.v65i0.19738, 2013.

494   Pandey, S. K. & Vinoj, V. Surprising changes in aerosol loading over india amid covid-19

495   lockdown. *Aerosol Air Qual. Res.* 21, 1–12, https://doi.org/10.4209/aaqr.2020.07.0466,

496   2021.

497   Qian, Y., Flanner, M. G., Leung, L. R. & Wang, W. Sensitivity studies on the impacts of

498   Tibetan Plateau snowpack pollution on the Asian hydrological cycle and monsoon

499   climate. *Atmos. Chem. Phys.* 11, 1929–1948, doi:10.5194/acp-11-1929-2011, 2011.

500   Rogelj, J. *Schaefferc M., Meinshausene M.,. Shindell D. T, Harec W., Klimontb Z. , Veldersh*

501   *G. J. M., Amannb M., and Schellnhuberr H.J.,* Disentangling the effects of CO2 and short

502   lived climate forcer mitigation. *Proc. Natl. Acad. Sci. U. S. A.* 111, 16325–16330,

503   https://doi.org/10.1073/pnas.1415631111, 2014.

504   Sabin, T., Krishnan, R., Vellore, R., Priya, P., Borgaonkar, H., Singh, B., Sagar, A. Droughts

505   and floods. Climate Change Over the Himalayas. Assessment Of Climate Change Over

506   The Indian Region. doi:10.1007/978-981-15-4327-2_11, 2020.

507   Santra, S. *Verma1 S., Fujita K, Chakraborty I, Boucher O., Takemura T., Burkhart John F.,*

508   *Matt F, and Sharma M.,* Simulations of black carbon (BC) aerosol impact over Hindu

509   Kush Himalayan sites: Validation, sources, and implications on glacier runoff. *Atmos.*

510   *Chem. Phys.* 19, 2441–2460, https://doi.org/10.5194/acp-19-2441-2019, 2019.

511   Sarangi, C. Qian Y., Rittger K., Bormann K.J., Liu Y., Wang H., Wan H., Lin G., and. Painter

512   T.H.*,* Impact of light-absorbing particles on snow albedo darkening and associated

513   radiative forcing over high-mountain Asia: high-resolution WRF-Chem modeling and

514   new satellite observations. *Atmos. Chem. Phys.* 19, 7105–7128,

515   https://doi.org/10.5194/acp-19- 7105-2019, 2019.

516 Sarangi, C., Qian, Y., Rittger, K., Ruby Leung, L., Chand, D., Bormann, K. J., and Painter, T.
517   H.: Dust dominates high-altitude snow darkening and melt over high-mountain Asia,
518   Nature Climate Change, 10, 1045-1051, 10.1038/s41558-020-00909-3, 2020.

519 Schultz, M. G., Stadtler S., Schröder S., Taraborrelli D., Franco B., Krefting J, Henrot A. et al.,
520   The chemistry-climate model ECHAM6.3-HAM2.3-MOZ1.0. *Geosci. Model Dev.* 11,
521   1695–1723, https://doi.org/10.5194/gmd-11-1695-2018, 2018.

522 Shafeeque, M. Arshad A., A Elbeltagi A., Sarwar A., Pham Q. B., S Khan S. N., l Dilawar A.
523   & Al-Ansari N., Understanding temporary reduction in atmospheric pollution and its
524   impacts on coastal aquatic system during COVID-19 lockdown: a case study of South
525   Asia.*Geomatics,   Nat.   Hazards   Risk   12,   560–580,*
526   https://doi.org/10.1080/19475705.2021.1885503, 2021.

527 Srivastava, A. K.. *Bhoyar P.D., K* 499 *anawade V. P., Devara P.C. S., Thomas A., Soni V.K.,*
528   Improved air quality during COVID-19 at an urban megacity over the Indo-Gangetic
529   Basin: From stringent to relaxed lockdown phases. *Urban Clim.* 36, 100791,
530   https://doi.org/10.1016/j.uclim.2021.100791, 2021.

531 Stevens, B., Giorgetta M., Esch M., Mauritsen T., Crueger T., Rast S., Salzmann M., Schmidt
532   H., Bader J., Block K., Brokopf R., Fast I., Kinne S., Kornblueh L., Lohmann U., Pincus
533   R., Reichler T., Roeckner E. Atmospheric component of the MPI-M earth system model:
534   ECHAM6. J. Adv. Model. Earth Syst. 5, 146–172, https://doi.org/10.1002/jame.20015,
535   2013.

536 Stier, P., Feichter J., Kinne S., Kloster S., Vignati E., Wilson J., Ganzeveld L., Tegen I., Werner
537   M., Balkanski Y. Schulz M., Boucher O., Minikin A., and Petzold A., Theaerosol-climate
538   model ECHAM5-HAM. *Atmos. Chem. Phys.* 5, 1125–1156, https://doi.org/10.5194/acp-
539   5-1125-2005, 2005.

Tegen, I., Neubauer D., Ferrachat S., Siegenthaler-Le Drian C, Bey, I., Schutgens N., Stier P., Watson-Parris D., et al., The global aerosol-climate model echam6.3-ham2.3 -Part 1: Aerosol evaluation. *Geosci. Model Dev.* 12, 1643–1677, https://doi.org/10.5194/gmd-12-1643-2019, 2019.

Textor , Schulz M, Guibert S., Kinne S., Balkanski Y., Bauer S., Berntsen T., Berglen T., Boucher O., Chin M., Dentener F, Diehl1 T., Easter R., Feichter H., Fillmore D., Ghan S., Ginoux P., Gong S., Grini A., Hendricks J. , Horowitz L., Huang P., Isaksen I., Iversen I, Kloster S., Koch D., Kirkevåg A., Kristjansson J. E., Krol M., Lauer A., Lamarque J. F., Liu X., Montanaro V., Myhre G., Penner J., Pitari G., Reddy5 S., Seland Ø., Stier P., Takemura T., and Tie X., Analysis and quantification of the diversities of aerosol life cycles within AeroCom. *Atmos. Chem. Phys.* 6, 1777–1813, https://doi.org/10.5194/acp-6-1777-2006, 2006.

Thind, P. S., Chandel, K. K., Sharma, S. K., Mandal, T. K. & John, S. Light-absorbing impurities in snow of the Indian Western Himalayas: impact on snow albedo, radiative forcing, and enhanced melting. *Environ. Sci. Pollut. Res.* 26, 7566–7578, https://doi.org/10.1007/s11356-019-04183-5, 2019.

Tiwari, S., Kar, S. C. & Bhatla, R. Snowfall and Snowmelt Variability over Himalayan Region in Inter-annual Timescale. *Aquat. Procedia* 4, 942–949,doi: 10.1016/j.aqpro.2015.02.118, 2015.

Usha, K. H., Nair, V. S. & Babu, S. S. Effect of aerosol-induced snow darkening on the direct radiative effect of aerosols over the Himalayan region. *Environ. Res. Lett.* 16, https://doi.org/10.1088/1748-9326/abf190, 2021.

Wester P., Mishra A., Mukherji A., S. A. B. The Hindu Kush Himalaya Assessment— Mountains, Climate Change, Sustainability and People. Springer Nature Switzerland AG, Cham. doi:https://doi.org/10.1007/978-3-319-92288-1, 2019.

565   Wood, L. R. Neumann K., Nicholson K.N., Bird B.W., Dowling C. B. and Sharma *S.*. Melting

566   Himalayan Glaciers Threaten Domestic Water Resources in the Mount Everest Region,

567   Nepal. *Front. Earth Sci.* 8, 1–8, https://doi.org/10.3389/feart.2020.00128, 2020.

568   Zhang, K. O'Donnell D., Kazil J., Stier P., Kinne S., Lohmann U., Ferrachat S., Croft B., Quaas

569   J, Wan H., Rast S., and Feichter J., The global aerosol-climate model ECHAMHAM,

570   version 2: Sensitivity to improvements in process representations. *Atmos. Chem.Phys.*

571   12, 8911–8949, https://doi.org/10.5194/acp-12-8911-2012, 2012.

572   *Zheng M.,*Impacts of COVID-19 on Black Carbon in Two Representative Regions in China:

573   Insights Based on Online Measurement in Beijing and Tibet. *Geophys. Res. Lett.* 48, 1–

574   11, 10.1029/2021GL092770, 2021.

575

576   **Acknowledgments**

577   The authors thank the staff of the High Power Computing Centre (HPC) in IITM, Pune, India,

578   for providing computer resources and the team members of MODIS for providing data. We

579   thank Sabur F. Abdullaev and Brent Holben for their efforts in establishing and maintaining

580   Dushanbe and Lahore AERONET sites respectively. Work done in the manuscript is not

581   supported by any funding agency.

582   Funding information

583   The manuscript is not funded.

584   **Author Contributions**

585   S.F. initiated the idea of the study. S.F. and B. H. performed model simulations. A.R. and A.

586   K. prepared Google based emission inventory. T.P.S., A.A., R.M. performed data analysis and

587   contributed in overall design. All authors contributed to discussions of the results and the

588   writing of the manuscript.

Data and code availability

The ECHAM-HAMMOZ model source code and all required input data are available to the scientific community according to the HAMMOZ Software License Agreement through the project website: https://redmine.hammoz.ethz.ch/projects/hammoz. The data that support the findings of this study are openly available in zenodo at http://doi.org/.../zenodo....

Competing Interests: The authors declare no competing interests.